Enhanced piezoelectricity and modified dielectric screening of 2-D group-IV monochalcogenides

Article *in* Physical Review B · November 2015

DOI: 10.1103/PhysRevB.92.214103 · Source: arXiv

3 authors, including:

Lidia C. Gomes
National University of Singapore
15 PUBLICATIONS **103** CITATIONS
SEE PROFILE

Antonio H. Castro Neto
National University of Singapore
470 PUBLICATIONS **33,785** CITATIONS
SEE PROFILE

Enhanced piezoelectricity and modified dielectric screening of 2-D group-IV monochalcogenides

Lídia C. Gomes, A. Carvalho, and A. H. Castro Neto
Centre for Advanced 2D Materials and Graphene Research Centre, National University of Singapore, 6 Science Drive 2, 117546, Singapore
(Dated: November 6, 2015)

We use first principles calculations to investigate the lattice properties of group-IV monochalcogenides. These include static dielectric permittivity, elastic and piezoelectric tensors. For the monolayer, it is found that the static permittivity, besides acquiring a dependence on the interlayer distance, is comparatively higher than in the 3D system. In contrast, it is found that elastic properties are little changed by the lower dimensionality. Poisson ratio relating in-plane deformations are close to zero, and the existence of a negative Poisson ratio is also predicted for the GeS compound. Finally, the monolayers shows piezoelectricity, with piezoelectric constants higher than that recently predicted to occur in other 2D-systems, as hexagonal BN and transition metal dichalcogenide monolayers.

PACS numbers: Valid PACS appear here

I. INTRODUCTION

Piezoelectric materials are used in very diverse fields of application as sensors, actuators, electric field generators, and in general in any other applications requiring a conversion between electrical and mechanical energy. Recently, the availability of piezoelectric nanowires and nanobelts inspired the design of a class of 'nanopiezotronic' devices which make use of both their piezoelectric and semiconducting properties.[1] These include, for example, nano-generators, field-effect transistors, and piezoelectric diodes. Lead-free biocompatible piezoelectric materials are also sought for, as components for biomedical devices.

Piezoelectric crystals can also be found amongst 2D materials. Some of these, like BN and 2H-stacked transition metal dichalcogenides, are centrosymmetric in bulk form, but loose the inversion symmetry if the number of layers is odd. Exfoliation of W and Mo dichalcogenide monolayers thus produces 2D piezoelectric crystals with strain-induced polarisation change in plane. This has been confirmed experimentally for MoS_2 by direct piezoresponse measurements and electrical characterisation of MoS_2 devices under strain[2]. For a few transition metal dichalcogenides, the in-plane d_{11} components of the piezoelectric tensor have been predicted to be superior to quartz.[3]

Here, we concentrate on yet another family of layered materials that are piezoelectric in the monolayer form. These are the group-IV monocalcogenides[4] SnS, GeS, SnSe and GeSe. Due to the hinge-like structure similar to that of black phosphorus[5] (Fig. 1), group-IV monocalcogenides are very ductile along the direction perpendicular to the zigzags, stretching in that direction when out-of-plane strain is applied. Since the direction perpendicular to the zigzags is also the main polar direction, this results in a very large piezoelectric coefficient, exceeding by at least one order of magnitude that of other known 2D piezoelectrics.

In addition, group-IV monochalcogenides present nearly vanishing or negative Poisson ratio. This is also a consequence of their anisotropic structure, as was recently reported[6] that a monolayer of black phosphorus (phosphorene) also possesses a negative Poisson ratio.

In this article, we use first principles calculations to predict the lattice response properties of this family of materials, comprising static dielectric constant, and elastic and piezoelectric constants.

A. Computational details

We use first-principles calculations to obtain structural properties of monochalcogenides. We employ a first-principles approach based on Kohn-Sham density functional theory (KS-DFT)[7], as implemented in the Vienna ab initio simulation package (VASP)[8,9], which was used for calculation of elastic, piezoelectric and static dielectric tensors. The core and valence electrons are treated with the projector-augmented wave (PAW) method[10].

The exchange correlation energy was described by the generalized gradient approximation (GGA) using the PBE[11] functional. For all materials, van der Waals interactions are taken into account by the method proposed by Tkatchenko and Scheffler[12] (TS), which presents a charge-density dependence of the dispersion coefficients and damping function. The Kohn-Sham orbitals were expanded in a plane-wave basis with a cutoff energy of 550 eV. The Brillouin-zone (BZ) was sampled using a Γ-centered 1×20×20 grid for the monolayers, following the scheme proposed by Monkhorst-Pack[13]. The results for bulk were obtained with a 6×16×16 grid. Structural optimization has been performed with a very stringent tolerance of 0.001 eV/Å.

For comparison, we also performed calculations with the Quantum ESPRESSO code,[14] in that case using Troullier-Martins pseudopotentials[15]. There was good agreement between the two codes whenever direct com-

parison could be established. All results shown were obtained with VASP, with exception of the Poisson ratio calculations, which were performed with QUANTUM ESPRESSO to take advantage of the implementation of geometry optimisation constraints.

The supercells are periodic in the monolayer plane and large vacuum regions (> 17 Å) are included to impose periodic boundary conditions in the perpendicular direction. Convergence tests with greater vacuum thickness were performed, and the values used are enough to avoid spurious interaction between neighboring images.

II. RESULTS

A. Structure

Bulk group-IV monochalcogenides SnS, SnSe, GeS and GeSe have an orthorhombic structure with eight atoms per unit cell, four of each species. They belong to the space group $Pnma$. This structure is also known as the α phase of SnS, a naturally occurring mineral[16]. The waved structure adopted by these materials is similar to that of black phosphorus, with which these compounds are isoelectronic. All atoms are three-fold coordinated and tetrahedral coordination results from the repulsion of the lone pairs. In the monolayer, the translational symmetry along the x direction is lost, and with it the inversion symmetry, and the resulting structure belongs to the $Pmn2_1$ space group. In this work, the axes system is chosen as the layers sit on the y-z plane, with the y axis parallel to the puckering direction, as shown in Fig. 1. The layers are stacked together along the x axis to form the bulk.

The calculated lattice parameters of these materials, for both bulk and monolayer, have been discussed in previous theoretical studies,[17–19], including our previous work at the GGA level[4]. Aware of the importance of van der Waals (vdW) interactions in layered materials, in this work we include these effect in order to obtain even more accurate structural properties of these materials. Table I presents the optimized lattice parameters for pure GGA and including vdW effects. Available experimental data for bulk SnS and SnSe are also included.

As should be expected, the most noticeable effects of vdW interactions in the structural parameters are on the lattice vector **a**, the one perpendicular to the plane of the layers in bulk. The inclusion of vdW forces results in values for **a** very close to the experimental data for bulk SnS and SnSe[20–22], with better results for the Tkatchenko-Scheffler method. The difference between PBE and vdW for monolayers is minor.

B. Static Dielectric Tensor

The static dielectric tensor ϵ is calculated from the force constant (**K**) and Born dynamical effective charges

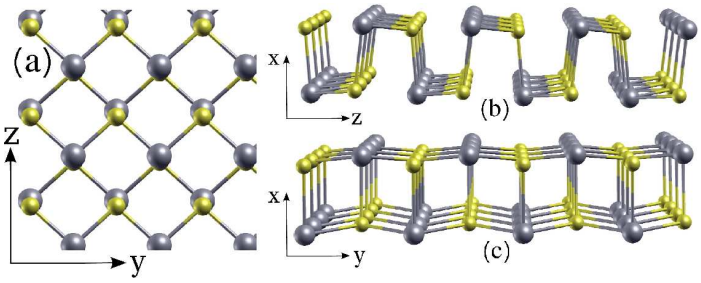

FIG. 1. (Color online) Structure of group-IV monochalcogenides. (a) Top-view and (b, c) side views of the monolayer unitcell, which are repeated along the x direction to obtain the bulk. The layers sit on the y-z plane, with the y axis parallel to the puckering direction.

		Monolayer		Bulk		
		b	**c**	**a**	**b**	**c**
SnS	PBE	4.07	4.24	11.37	4.02	4.35
	vdW-TS	4.08	4.25	11.12	4.00	4.27
	Expt.	-	-	11.20	3.98	4.33
SnSe	PBE	4.30	4.36	11.81	4.22	4.47
	vdW-TS	4.27	4.37	11.58	4.20	4.47
	Expt.	-	-	11.50	4.15	4.44
GeS	PBE	3.68	4.40	10.81	3.68	4.40
	vdW-TS	3.73	4.30	10.41	3.67	4.34
GeSe	PBE	3.99	4.26	11.31	3.91	4.45
	vdW-TS	4.00	4.22	10.93	3.90	4.39

TABLE I. Optimized lattice parameters (in Å) for α phase of SnS, SnSe, GeS, GeSe. We present results for PBE-GGA and including vdW by Tkatchenko-Scheffler (TS) method. Experimental data for bulk SnS[20,21] and SnSe[22] are also presented.

(BEC) (**Z**) tensors:[23]

$$\epsilon_{ij} = \epsilon_{ij}^{\infty} + V_0^{-1} Z_{mi} (K^{-1})_{mn} Z_{nj}. \quad (1)$$

The tensors **K** and **Z** are second derivative response functions and are calculated using density functional perturbation theory.

The electronic contribution ϵ_{ij}^{∞}, or ion-clamped static dielectric tensor, has been given in Ref. 4. Here, we will concentrate on the lattice contribution, which for static electric fields, exceeds the electronic contribution.

For orthorhombic materials, the dielectric permittivity tensor has the form

$$\epsilon_{ij} = \begin{bmatrix} \epsilon_1 & 0 & 0 \\ 0 & \epsilon_2 & 0 \\ 0 & 0 & \epsilon_3 \end{bmatrix}, \quad (2)$$

where we have contracted a two-index into a one-index notation. The values calculated for bulk are given in Tab. II. While for the tin chalcogenides the calculated values are in excellent agreement with estimates obtained from comparing the LO-TO splitting of the vibrational bands with the dielectric constants obtained from reflectivity data, for the germanium chalcogenides there is some discrepancy. This can be due to many factors, including crystal quality. In particular, the dielectric response along the **x** axis is difficult to measure, explaining the range of variation of the measured values.

For two-dimensional materials, the dielectric constant is not well defined, depending on the interlayer distance L as[24–26]

$$\epsilon_i = \delta_i + \frac{4\pi\chi_i^{2\mathrm{D}}}{L}, \tag{3}$$

where the 2D polarizability $\chi^{2\mathrm{D}}$ (which includes both ionic and electronic contributions) is a constant and $\alpha, \beta = 2, 3$, in accordance with our convention of the layers in the $y-z$ plane. The $1/L$ dependence on the interlayer spacing of the electronic contribution to the susceptibility in the 2D systems has been verified in previous works.[24–26]. In this work, we verified that the same behaviour applies to the ionic contribution. In practice, this can be calculated using the same method as bulk (Eq. 1) but replacing the volume by the area. The ionic contribution to $\chi^{2\mathrm{D}}$ for the monolayers is given in Tab. II.

For comparison, if the interlayer distance L in the monolayer is taken to be the same as in bulk, the vdW-TS calculations for SnS results in static ionic contributions to the permittivity with values 61 and 23, respectively, along the y direction, and 39 and 14, respectively, along the z direction, showing an increase of ~ 2.5 times when comparing the 2D and 3D systems. For SnSe and GeSe the ionic contribution to ϵ in monolayer reaches values three to four times higher than in their respective bulk forms. In the other hand, GeS presents just slightly higher values for ϵ from bulk to monolayer. The increase in the screening for SnS, SnSe and GeSe can be explained by two factors: (i) increase in Born effective charges (BEC) and (ii) softening of polar modes due to the absence of interlayer binding. The increase in the BEC can be as higher as 28% for SnS, SnSe and GeSe, while for GeS **Z** differs by less than 3%. To have a better understanding of the contribution of lattice vibrational mode softening to the increase of the static dielectric constant, we consider the contribution of different modes to the components of the static dielectric tensor, by writing ϵ_{ij} as in Ref. 31 and 32:

$$\epsilon_{ij} = \epsilon_{ij}^{\infty} + \frac{4\pi}{V_0}\sum_m \frac{S_{m,ij}}{\omega_m^2} \tag{4}$$

where V_0 is the volume of the cell. $S_{m,ij}$ is called the mode-oscillator strength of the ω_m mode along the $i, j(=x, y, z)$ directions of the material and it is related to the eigendisplacements $U_m(\kappa i)$ and Born effective charge tensors $Z^*_{\kappa,ii'}$ by:

$$S_{m,ij} = \left(\sum_{\kappa i'} Z^*_{\kappa,ii'} U^*_{m\mathbf{q}=0}(\kappa i')\right)\left(\sum_{\kappa' j'} Z^*_{\kappa',jj'} U_{m\mathbf{q}=0}(\kappa' j')\right). \tag{5}$$

κ is the index for the ions in the primitive cell. The ionic contribution to ϵ is then given by the second term in the right side of Eq. 4. The expression for $S_{m,\alpha\beta}$ shows that and increase in the BEC increases the contribution of the ionic part of ϵ. However, the dominant contribution comes from the ω_m modes. In Tab. III we present the frequency of the modes with major contribution to the static dielectric constant for monolayer and bulk monochalcogenides, along the in-plane directions. For all materials, just one mode contributes significantly to the yy component of ϵ, while there are two modes which contributes almost equally to the zz components in bulk SnS and monolayer and bulk SnSe and GeSe. A significant softening of the contributing modes occurs when going from 3D to 2D forms, probably due to the lack of interaction with upper and bottom layers, observed in bulk. SnSe presents the largest softening in the contributing modes, with $\omega_m^{3D}/\omega_m^{2D} = 1.9$ along the y direction up to $\omega_m^{3D}/\omega_m^{2D} = 2.5$ along z. GeS, however, presents the smallest softening of the modes, where we have $\omega_m^{3D}/\omega_m^{2D} = 1.1$ and 1.5 for the contribution to the yy and zz components of ϵ.

C. Elastic Constants and Poisson ratio

a. Elastic constants: The elastic constant (stiffness) tensor is defined in the linear regime by Hooke's law:

$$\sigma_i = C_{ij}\varepsilon_j, \tag{6}$$

where σ and ε are the stress and strain tensors, respectively, C_{ij} are the elastic constants. In this equation, and the following, there is an implicit sum over repeated indexes. Numerically, the elastic constants are easily determined using the equation of state. The change in the total energy $E(V_0)$ of a system due to an external strain (ε) is given by

$$E(V_0, \varepsilon) = E(V_0) + \frac{V_0}{2}C_{ij}\varepsilon_i\varepsilon_j, \tag{7}$$

where V_0 is the volume of the unstrained material. Here, the electric field term vanishes because of the periodic boundary conditions ($d\vec{E} = 0$). For the monolayer system, the area (A_0) should figure instead. However, to facilitate the comparison with 3D systems and previous calculations,[33] we use an effective thickness d_0. The most obvious choice is to take d_0 to be the distance between the layers in bulk, as is common practice in graphene[34].

		Monolayer				Bulk						
									Expt.			
		χ_2^{2D}	χ_3^{2D}	ϵ_2	ϵ_3	ϵ_1	ϵ_2	ϵ_3	ϵ_1	ϵ_2	ϵ_3	
SnS	PBE	35.8	21.5	78.0	50.1	14.9	31.7	18.3	16±6	32±7	18±6	Ref. (a)
	vdW-TS	27.3	17.2	61.7	39.0	27.5	22.6	13.8	18.4	34.5	20.7	Ref. (d)
SnSe	PBE	73.6	26.4	156.5	56.0	21.3	39.1	12.1	26±7	45±8	32±7	Ref. (a)
	vdW-TS	76.4	37.7	165.7	82.0	25.7	32.0	15.9	17.5	32.5	18.5	Ref. (d)
GeS	PBE	5.3	3.1	12.4	7.4	6.8	11.8	7.6	20.0	17.5	10.3	Ref. (b)
	vdW-TS	7.1	3.6	16.1	8.6	16.7	12.9	8.5	10.6	14.0	10.6	Ref. (d)
GeSe	PBE	24.0	7.7	53.3	17.1	6.9	12.3	5.7	11.3	8.5	3.2	Ref. (c)
	vdW-TS	28.6	10.1	65.7	24.3	14.3	15.7	7.7	9.7	12.5	9.6	Ref. (d)

TABLE II. Ionic contributions to the 2D polarizability χ_2^{2D} and χ_3^{2D}, macroscopic static dielectric tensor components ϵ_2 and ϵ_3 for y and z directions of the monolayers, and ϵ_1, ϵ_2 and ϵ_3 for x, y and z directions of bulk. Results for PBE-GGA and taking into account van der Walls interactions are included. Our calculations for the bulk can be compared to experimental values from the previous works: (a) Ref. 27, (b) Ref. 28, (c) Ref. 29, (d) Ref. 30.

	yy		zz	
	Monolayer	Bulk	Monolayer	Bulk
SnS	104	158	62	102 / 189
SnSe	53	102	56 / 78	132 / 86
GeS	180	207	77	116
GeSe	94	145	137 / 76	184 / 87

TABLE III. Modes (cm^{-1}) at $\mathbf{q}$=0 with largest contribution to the static dielectric tensor as defined in Eq. 4. The values presented in this table are obtained considering vdW interactions and do not take into account LO-TO splitting effects.

Symmetry imposes restrictions on the number of non-zero components C_{ij}. Both for bulk and monolayer there are nine independent nonvanishing elements C_{ij} (in Voigt notation):

$$C_{ij} = \begin{bmatrix} C_{11} & C_{12} & C_{13} & 0 & 0 & 0 \\ C_{12} & C_{22} & C_{23} & 0 & 0 & 0 \\ C_{13} & C_{23} & C_{33} & 0 & 0 & 0 \\ 0 & 0 & 0 & C_{44} & 0 & 0 \\ 0 & 0 & 0 & 0 & C_{55} & 0 \\ 0 & 0 & 0 & 0 & 0 & C_{66} \end{bmatrix} \quad (8)$$

However, we will consider that the monolayers are ideal 2D systems, with only in-plane stress. This excludes the elastic constants coupling ε_i to σ_6 and σ_5, (this is equivalent to σ_{12} and σ_{13}). Since in the absence of an external torque the σ tensor is symmetrical, the only relevant elements are (in Voigt's notation) C_{22}, C_{33}, C_{23} and C_{44}.

The elastic constants for the monolayer were obtained from Eq. 6, applying finite distortions to the supercell. The stress components σ_{2i} and σ_{3i} are calculated using the effective thickness d_0 to define the lateral area of the layers. We have calculated C_{ij} both in clamped-ion and relaxed-ion conditions, by fixing the atomic coordinates or allowing them to relax, respectively, for each distortion of the lattice vectors. The results for bulk and monolayer group-IV monochalcogenides are presented in Table IV, for calculations with and without vdW effects. Using the definition of d_0, the elastic constants are of the same order of magnitude for monolayer and bulk. In most cases though, they are slightly higher for the bulk for both relaxed and clamped-ion coefficients, indicating that the monolayers are less stiff for in-plane deformations. The main effects of vdW interactions in bulk are observed in the elastic constant components related to the x direction of the materials (those with index $1j$, j=1, 2, 3 as well as 55 and 66). The C_{11} constants are the most affected by the vdW forces, as expected, and differences up to 50% are observed when compared to the PBE-GGA results.

Figure 2 shows the total energy versus strain along the y and z directions for a SnSe monolayer. The quadratic dependence of energy to the applied strain and the anisotropy between the perpendicular in-plane directions of the layer is given by

$$\Delta E(V,\varepsilon) = \frac{V_0}{2}\left(C_{22}\varepsilon_2^2 + C_{33}\varepsilon_3^2\right) + V_0 C_{23}\varepsilon_2\varepsilon_3 \quad (9)$$

where $\Delta E(V,\varepsilon) = E(V,\varepsilon) - E(V_0,\varepsilon=0)$ and $C_{32} = C_{23}$. The results for SnS, GeS and GeSe are very similar, differing only in the ratio between elastic constants.

It is also noteworthy that C_{22} (the elastic constant for the zig-zag direction) is much lower for group-IV monochalcogenides than for black-phosphorus (18.6 $\times 10^{10}$ N/m^2), in contrast with other elastic constant elements which are little changed[35].

			Monolayer								
			C_{11}	C_{22}	C_{33}	C_{12}	C_{13}	C_{23}	C_{44}	C_{55}	C_{66}
SnS	PBE	C-i	-	9.59	8.81	-	-	5.68	5.50	-	-
		R-i	-	7.59	3.67	-	-	3.19	3.44	-	-
	vdW-TS	C-i	-	9.65	9.29	-	-	5.70	5.25	-	-
		R-i	-	7.72	3.85	-	-	2.68	2.81	-	-
SnSe	PBE	C-i	-	7.90	7.26	-	-	4.54	4.81	-	-
		R-i	-	6.92	3.32	-	-	2.77	2.32	-	-
	vdW-TS	C-i	-	5.68	5.34	-	-	2.96	3.28	-	-
		R-i	-	5.04	2.89	-	-	1.83	1.80	-	-
GeS	PBE	C-i	-	9.51	8.92	-	-	6.08	5.41	-	-
		R-i	-	8.48	2.82	-	-	4.00	3.44	-	-
	vdW-TS	C-i	-	9.41	9.25	-	-	6.17	5.52	-	-
		R-i	-	8.26	3.02	-	-	3.93	3.49	-	-
GeSe	PBE	C-i	-	9.78	8.46	-	-	5.34	6.00	-	-
		R-i	-	8.87	3.59	-	-	3.44	4.10	-	-
	vdW-TS	C-i	-	10.19	9.37	-	-	5.42	6.04	-	-
		R-i	-	9.19	4.41	-	-	3.40	3.81	-	-
			Bulk								
			C_{11}	C_{22}	C_{33}	C_{12}	C_{13}	C_{23}	C_{44}	C_{55}	C_{66}
SnS	PBE	C-i	12.12	9.53	8.31	2.45	2.56	5.51	5.29	2.56	2.43
		R-i	4.85	7.99	3.42	1.31	1.80	3.16	3.47	1.95	2.00
	vdW-TS	C-i	12.15	9.68	8.79	2.64	3.07	5.59	5.37	3.15	2.74
		R-i	6.59	7.70	3.84	1.86	2.66	2.80	3.24	2.87	2.50
SnSe	PBE	C-i	10.99	8.39	7.61	1.76	2.03	5.09	5.20	1.93	1.77
		R-i	4.35	6.93	3.48	0.74	1.23	2.99	3.32	1.37	1.07
	vdW-TS	C-i	11.72	9.30	8.29	1.87	2.44	5.23	5.40	2.44	1.97
		R-i	6.09	7.49	4.27	0.99	2.12	2.86	3.29	2.09	1.24
GeS	PBE	C-i	12.40	10.47	8.83	2.79	2.67	6.00	5.75	3.18	2.93
	R-i	3.78	8.96	3.02	0.97	0.72	3.31	3.65	1.69	1.73	
	vdW-TS	C-i	12.84	10.93	9.48	2.72	2.91	5.94	6.13	3.61	3.35
		R-i	5.31	8.94	3.41	1.11	1.44	2.81	3.76	2.90	2.51
GeSe	PBE	C-i	12.14	10.47	8.59	1.98	2.05	6.45	6.52	2.43	2.42
		R-i	3.20	8.72	3.75	0.29	0.82	3.91	3.93	1.15	0.96
	vdW-TS	C-i	12.53	10.02	8.63	1.73	2.22	5.64	5.67	2.92	2.44
		R-i	4.16	8.06	3.85	0.26	1.38	3.05	3.50	2.08	0.88

TABLE IV. Calculated clamped-ion (C-i) and relaxed-ion (R-i) components of the elastic tensor C_{ij} for bulk and monolayer. The elastic constants for the monolayer assume an effective layer thickness $d_0 = a/2$ to allow direct comparison with bulk. All values are given in 10^{10} N/m^2.

b. Young modulus and Poisson ratio The Young modulus and Poisson ratio are derived mechanical properties that can give direct information on how a system

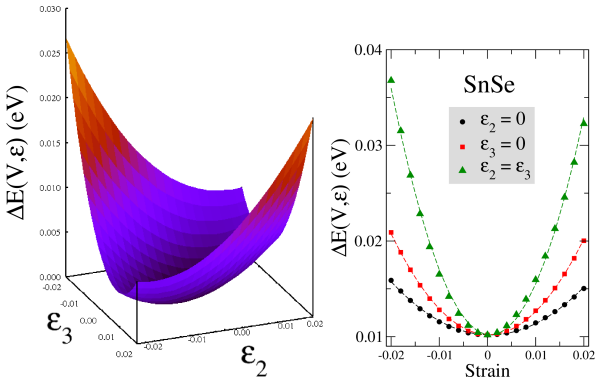

FIG. 2. (Color online) The three-dimensional surface plot of total energy (in eV) versus uniaxial strain along y and z directions of a SnSe monolayer. Projections on the $\varepsilon_2 = 0$, $\varepsilon_3 = 0$ and $\varepsilon_2 = \varepsilon_3$ planes show the quadratic dependence of the energy of the system to the applied strain, from where the elastic constants can also be calculated.

behaves under uniaxial stress ie. when $\sigma_i \neq 0$ and $\sigma_j = 0$ for all $j \neq i$. Here, we calculate these moduli to highlight the role of anisotropy on the mechanical response of group-IV monochalcogenides.

We define the Young modulus as

$$Y^i = \frac{\partial \sigma_i}{\partial \varepsilon_i}. \tag{10}$$

Since the materials in consideration here are orthorhombic, and the choice of principal direction is arbitrary, i can be any of the principal directions of the crystal. Similarly, we define multiple Poisson ratios ν_{ij}, corresponding to the negative ratio of the strain response at a i direction to the strain applied along a transversal j direction:

$$\nu_{ij} = -\frac{\partial \varepsilon_i}{\partial \varepsilon_j}. \tag{11}$$

for $i \neq j$.

In order to calculate Poisson ratio and Young modulus of monolayer monochalcogenides, according to Eq. 10 and 11, strains from -6% to 6% were applied in the in-plane and out-of-plane directions of the layers. As the elastic constants of single-layers are not considerable modified by introduction of vdW effects (Tab. IV), we include only the results for calculations performed with the PBE-GGA functional.

Most of the materials have a positive Poisson ratio, which means that when a compressive strain is applied along one direction, the others expand. Conversely, if the material is stretched along one direction, it will compress along the perpendicular directions. This due to the materials' tendency to conserve their volume. However, since group-IV monochalcogenides are very anisotropic, the values for the Poisson ratio vary greatly for different combination of directions i, j.

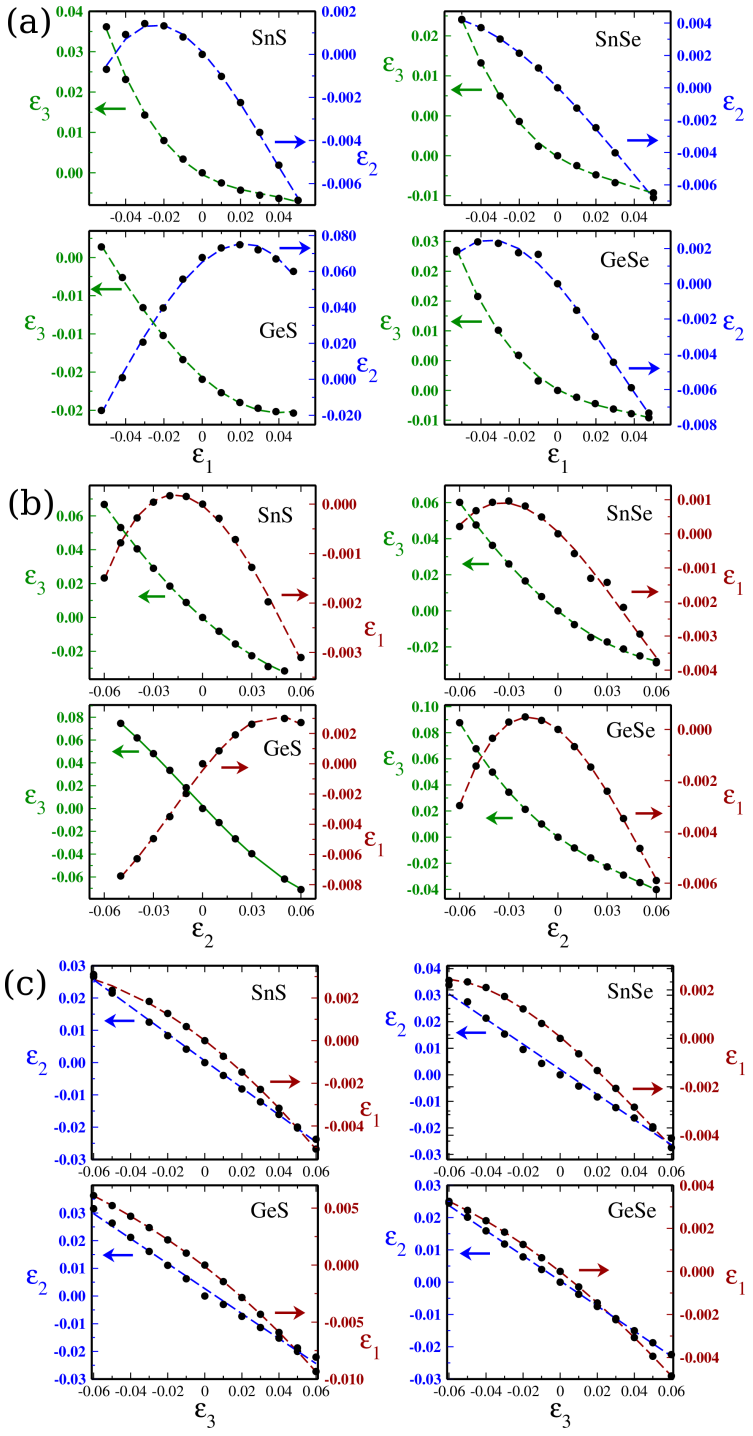

FIG. 3. (Color online) Response of monolayer monochalcogenides under uniaxial stress along (a) $\hat{x}$, (b) $\hat{y}$ and (c) $\hat{z}$ directions of the layers. Strain components for the directions perpendicular to the external force are plotted as a function of the strain component along the direction of the external force.

This is apparent in Figure 3, which illustrates the response of the monolayers under uniaxial stress. Firstly, it is clear that the linear region where the Young modulus

and Poisson ratio given by Eqs. 10 and 11 are constant is quite narrow, in some cases less than 2% strain.

In particular, if $i = 1$ or $j = 1$, the Poisson ratio is very close to zero, indicating that distortion along the in-plane directions and the direction perpendicular to the plane are practically decoupled. A very interesting exception is found in GeS: this is the only material in group-IV monochalcogenides that shows a negative linear Poisson ratio in the out of plane x direction. The calculated value of $\nu_{12} = -0.137$ for GeS is about five times larger than the value calculated for phosphorene in Ref. 36, which report $\nu_{12} = -0.027$ for this material.

In contrast, the ratios ν_{23} and ν_{32} for in-plane uniaxial stress are in the ranges 0.3-0.5 and 0.7-1.6. The Poisson ratio is intrinsically linked with the anisotropy. Plotting the Poisson ratio against the anisotropy of the monolayer crystals (b/c), it becomes evident why GeS departs from the other materials (Fig. 4). Amongst all four materials, GeS has the smallest b/c ratio, and is located far away from GeSe, SnS and SnSe. This behavior is more evident in the plot of ν_{21} and ν_{31} (left panel in Fig. 4), obtained by applying uniaxial strain in the out-of plane x direction.

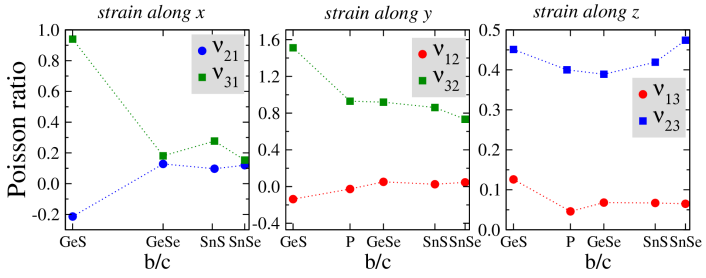

FIG. 4. (Color online) Poisson ratio versus the degree of anisotropy, given by the ratio between in-plane lattice constants b and c, for monolayer crystals. The values for phosphorene (P) taken from Ref. 36 are also included.

D. Piezoelectric tensor

Non-centrosymmetric crystals display a change of polarisation P_i under mechanical stress,

$$P_i = d_{ij}\sigma_j. \tag{12}$$

Equation 12 shows that application of a stress σ_j along the j-direction of a piezoelectric material induces a change of polarisation of magnitude P_i in its i-direction. P_i is related to σ_j by a piezoelectric tensor with components d_{ij}. This is known as the direct piezoelectric effect. In the same way, the converse piezoelectric effect occurs when a strain ε is induced in a material under an external electric field. The converse effect can be written:

$$\varepsilon_j = d_{ij}E_i, \tag{13}$$

where E_i is the component of the applied electric field in the i direction. The piezoelectric coefficients d_{ij} in Eqs. 12 and 13 are the same, and the proof of such equality is based on thermodynamical arguments[38]. In addition, other piezoelectric coefficients can be defined, for example e_{ij}, that directly relates E and σ by:

$$e_{ij} = -\frac{\partial\sigma_j}{\partial E_i} = \frac{\partial P_i}{\partial\varepsilon_j}. \tag{14}$$

For a constant electric field, the piezoelectric tensors d_{ij} and e_{ij} are related via the elastic tensor C_{ij} as:

$$e_{ij} = \sum_{k=1}^{6} d_{ik}C_{kj}. \tag{15}$$

However, in the case of a 2D system it is more meaningful to define a 2D polarisation per unit area, P_i^{2D}. Thus, we redefine e_{ij}^{2D}

$$e_{ij}^{2D} = \frac{\partial P_i^{2D}}{\partial\varepsilon_j}. \tag{16}$$

The number of non-zero coefficients e_{ij}^{2D} are completely defined by the symmetry of the system. The layered group-IV monochalcogenides are centrosymmetric in bulk (and even-numbered layers) and therefore are not piezoelectric. However, single layers belong to the polar space group $Pmn2_1$. In this space group, there are five non-zero piezoelectric constants: e_{15}^{2D}, e_{24}^{2D}, e_{31}^{2D}, e_{32}^{2D}, and e_{33}^{2D}, where we use the Voigt's notation[38] with 1, 2 and 3 corresponding to x, y and z directions, respectively.[39] As for the calculation of the elastic constants, we consider only in-plane strain components for computation of the e_{ij}^{2D} constants, which limit our discussion to e_{32}^{2D}, e_{33}^{2D} and e_{24}^{2D}. The calculated values are presented in Table VI.

$$e_{ij}^{2D} = \begin{bmatrix} 0 & 0 & 0 & 0 & e_{15}^{2D} & 0 \\ 0 & 0 & 0 & e_{24}^{2D} & 0 & 0 \\ e_{31}^{2D} & e_{32}^{2D} & e_{33}^{2D} & 0 & 0 & 0 \end{bmatrix} \tag{17}$$

For the best of our knowledge, there is still no experimental data on the piezoelectric properties of odd-number layers group-IV monochalcogenides. However, we take for comparison single layer TMDCs and h-BN, of which piezoelectric coefficients have been theoretically calculated[3], and object of recent experimental measurements[40].

Similar to h-BN and TMDC,[3] the piezoelectric elements e_{32}, e_{33} and e_{24} of group IV monochalcogenides are enhanced as we move downward in the periodic table. The value of e_{33} (for both relaxed and clamped-ion case) seems also to be directly related to the degree of anisotropy of the materials as given by the ratio between in-plane lattice parameters b/c.

For SnS and SnSe, e_{33} is one order of magnitude higher than for other known 2D piezoelectric materials. This

	ε_1		ε_2		ε_3					
	ν_{21}	ν_{31}	ν_{12}	ν_{32}	ν_{13}	ν_{23}	b/c	Y_1	Y_2	Y_3
SnS	0.097	0.277	0.025	0.861	0.067	0.419	0.97	32.4	15.1	8.7
SnSe	0.120	0.153	0.046	0.733	0.065	0.474	0.99	30.4	16.2	11.3
GeS	-0.214	0.940	-0.137	1.512	0.126	0.451	0.84	26.8	7.8	2.2
GeSe	0.128	0.181	0.051	0.919	0.068	0.389	0.94	30.2	15.9	7.9
P	-	-	-0.027	0.930	0.046	0.400	0.88	44.0	166.0	-

TABLE V. Poisson ratio and Young modulus (in GPa) for the monolayers monochalcogenides. The data for monolayer phosphorene from Refs. 36 and 37 are included for comparison. b/c is the ratio between in-plane lattice parameters.

		clamped-ion			relaxed-ion		
		e_{32}^{2D}	e_{33}^{2D}	e_{24}^{2D}	e_{32}^{2D}	e_{33}^{2D}	e_{24}^{2D}
SnS	PBE	-4.73	0.29	-4.39	0.76	23.36	15.70
	vdW-TS	-5.01	0.47	-4.75	2.27	18.94	15.54
SnSe	PBE	-4.89	0.53	-4.67	4.42	24.18	28.17
	vdW-TS	-4.67	0.58	-4.29	6.73	30.25	30.82
GeS	PBE	-6.69	-1.25	-7.10	-4.97	7.28	0.37
	vdW-TS	-6.89	-0.81	-7.08	-4.64	8.83	2.05
GeSe	PBE	-7.16	-0.26	-7.37	-3.00	13.26	8.25
	vdW-TS	-7.11	0.35	-7.20	-1.48	16.95	12.48
h-BN		-3.71	3.71	-	-1.38	1.38	-
MoS_2		-3.06	3.06	-	-3.64	3.64	-
$MoTe_2$		-2.98	2.98	-	-5.43	5.43	-

TABLE VI. Nonzero ion-clamped and relaxed-ion piezoelectric coefficients (10^{-10} C/m). The tensor components are calculated according to $e_{ij}^0 = -\frac{\partial \sigma_i}{\partial E_j}$, where the values for the other 2D materials h-BN, MoS_2 and $MoTe_2$ are taken from Ref.[3] and included for comparison.

element relates the polarisation along the z direction, the polar direction of the crystal, with the strain along the same direction. Since, as we have discussed before, this structure is extremely ductile along the z direction, the corresponding piezoelectric response is very large.

Our results agree with those recently reported in Ref. 41, which also investigates piezoelectric properties of monochalcogenides. Although there are some small quantitative discrepancies, the overall qualitative results between both works are in quite good agreement.

It is also instructive to compare the piezoelectric coefficients of group-IV monochalcogenides with typical 3D piezoelectric materials. Employing once again the definition of an effective tickness d_0, we obtain $e_{33} = 4.11$, 4.26, 1.36 and 2.37 C/m^2, for SnS, SnSe, GeS and GeSe, respectively. These coefficients are one to two orders of magnitude higher than the piezoelectric coefficients of the α quartz and four of its homeotypes MXO_4 (M = Al, Ga, Fe; X=P,As)[42].

III. CONCLUSIONS

The group-VI monochalcogenides SnS, SnSe, GeS and GeSe have an ortorhombic structure similar to phosphorene. This structure results in in-plane anisotropy of the static permittivity, elastic constants and piezoelectric coefficients. In this study, we investigated those properties both for monolayer and bulk systems by including van der Waals effects, highlighting the differences resulting from the lower dimensionality. The electric susceptibility in the 2D systems is known to have an $1/L$ dependence on the interlayer spacing.[24] This has been verified for electronic contribution to the low-frequency susceptibility.[25] In this work, we verified numerically that the same applies to the ionic contribution. However, if we extrapolate the ionic contribution to the 2D permittivity to $L = a/2$, where $a/2$ is the inter-layer spacing in bulk, we notice a great enhancement for SnS, SnSe and GeSe. This is mainly due to the larger softening of the modes in the 2D systems, but also partially accounted for the effective Born charges in the 2D material.

In contrast, elastic constants remain nearly unchanged in monolayer, compared to bulk, if an equivalent volume of material is considered. The most remarkable amongst the elastic properties of group-VI monochalcogenides is the Poisson ratio. The Poisson ratio ν_{12} and ν_{21}, relating strain and uniaxial strain for the direction perpendicu-

lar to the plane and the armchair in-plane direction are very small or even negative for GeS, the most anisotropic amongst the four materials.

Finally, while in bulk the presence of inversion symmetry forbids piezoelectricity, in monolayer there is one polar direction coinciding with the C_2 axis (z). Piezoelectric constants are higher than that recently predicted to occur in other 2D-systems, as hexagonal BN and transition metal dichalcogenide crystals.

ACKNOWLEDGEMENTS

This work was supported by the National Research Foundation, Prime Minister Office, Singapore, under its Medium Sized Centre Programme and CRP award "Novel 2D materials with tailored properties: beyond graphene" (Grant number R-144-000-295-281). The first-principles calculations were carried out on the GRC high-performance computing facilities.

[1] Z.L. Wang. *Advanced Materials*, 19:889–892, 2007.
[2] Wenzhuo Wu, Lei Wang, Yilei Li, Fan Zhang, Long Lin, Simiao Niu, Daniel Chenet, Xian Zhang, Yufeng Hao, Tony F. Heinz, James Hone, and Zhong Lin Wang. *Nature*, 514:470, 2014.
[3] Karel-Alexander N. Duerloo, Mitchell T. Ong, and Evan J. Reed. *The Journal of Physical Chemistry Letters*, 3:2871, (2012).
[4] Lídia C. Gomes and A. Carvalho. *Phys. Rev. B*, 92:085406, 2015.
[5] Zhen Zhu, Jie Guan, Dan Liu, and David Tomnek. *ACS Nano*, 9:8284, 2015.
[6] Jin-Wu Jiang and Harold S. Park. *Nat Commun*, 5, 2014.
[7] W. Kohn and L. J. Sham. *Phys. Rev.*, 140:A1133–A1138, 1965.
[8] G. Kresse and J. Furthmller. *Computational Materials Science*, 6:15–50, 1996.
[9] G. Kresse and J. Furthmüller. *Phys. Rev. B*, 54:11169–11186, 1996.
[10] P. E. Blöchl. *Phys. Rev. B*, 50:17953–17979, 1994.
[11] John P. Perdew, Kieron Burke, and Matthias Ernzerhof. *Phys. Rev. Lett.*, 77:3865–3868, 1996.
[12] Alexandre Tkatchenko and Matthias Scheffler. *Phys. Rev. Lett.*, 102:073005, 2009.
[13] Hendrik J. Monkhorst and James D. Pack. *Phys. Rev. B*, 13:5188–5192, 1976.
[14] Paolo Giannozzi et al. *Journal of Physics: Condensed Matter*, 21(39):395502, 2009.
[15] N. Troullier and José Luís Martins. *Phys. Rev. B*, 43:1993–2006, 1991.
[16] Aron Walsh and Graeme W. Watson. *Phys. Rev. B*, 70:235114, 2004.
[17] Georgios A. Tritsaris, Brad D. Malone, and Efthimios Kaxiras. *Journal of Applied Physics*, 113, 2013.
[18] Julien Vidal, Stephan Lany, Mayeul dAvezac, Alex Zunger, Andriy Zakutayev, Jason Francis, and Janet Tate. *Applied Physics Letters*, 100(3), 2012.
[19] Sebahaddin Alptekin and Murat Durandurdu. *Solid State Communications*, 150:870 – 874, 2010.
[20] H Wiedemeier and H G Schnering. *Z Kristallogr.*, 156 (143), 1981.
[21] L Ehm, K Knorr, P Dera, A Krimmel, P Bouvier, and M Mezouar. *Journal of Physics: Condensed Matter*, 16:3545, 2004.
[22] I. Lefebvre, M. A. Szymanski, J. Olivier-Fourcade, and J. C. Jumas. *Phys. Rev. B*, 58:1896–1906, 1998.
[23] Xifan Wu, David Vanderbilt, and D. R. Hamann. *Phys. Rev. B*, 72:035105, Jul 2005.
[24] Pierluigi Cudazzo, Ilya V. Tokatly, and Angel Rubio. *Phys. Rev. B*, 84:085406, 2011.
[25] Timothy C. Berkelbach, Mark S. Hybertsen, and David R. Reichman. *Phys. Rev. B*, 88:045318, 2013.
[26] Douglas Warschauer. *Journal of Applied Physics*, 34:1853–1860, 1963.
[27] H. R. Chandrasekhar, R. G. Humphreys, U. Zwick, and M. Cardona. *Phys. Rev. B*, 15:2177–2183, 1977.
[28] J. D. Wiley, W. J. Buckel, and R. L. Schmidt. *Phys. Rev. B*, 13:2489–2496, 1976.
[29] H.R. Chandrasekhar and U. Zwick. *Solid State Communications*, 18:1509 – 1513, 1976.
[30] Li-Ming Yu, A. Degiovanni, P. A. Thiry, J. Ghijsen, R. Caudano, and Ph. Lambin. *Phys. Rev. B*, 47:16222–16228, 1993.
[31] Xavier Gonze and Changyol Lee. *Phys. Rev. B*, 55:10355–10368, 1997.
[32] G.-M. Rignanese, X. Gonze, and Alfredo Pasquarello. *Phys. Rev. B*, 63:104305, 2001.
[33] Qun Wei and Xihong Peng. *Applied Physics Letters*, 104:251915, 2014.
[34] M Klintenberg, S Lebegue, C Ortiz, B Sanyal, J Fransson, and O Eriksson. *Journal of Physics: Condensed Matter*, 21:335502, 2009.
[35] S. Appalakondaiah, G. Vaitheeswaran, S. Lebègue, N. E. Christensen, and A. Svane. *Phys. Rev. B*, 86:035105, 2012.
[36] Jin-Wu Jiang and Harold S. Park. *Nat Commun*, 5, 2014.
[37] Qun Wei and Xihong Peng. *Applied Physics Letters*, 104, 2014.
[38] J F Nye. *Physical Properties of Crystals*. 1957.
[39] Note1. According to Voigt's notation, the indices are contracted according to 11 → 1, 22 → 2, 11 → 1, 33 → 3, 23(32) → 4, 13(31) → 5, 12(21) → 6, so that $e_{16}^{2D} = e_{112}^{2D} = e_{121}^{2D}$, $e_{25}^{2D} = e_{223}^{2D} = e_{232}^{2D}$, and so on.
[40] Wenzhuo Wu, Lei Wang, Yilei Li, Fan Zhang, Long Lin, Simiao Niu, Daniel Chenet, Xian Zhang, Yufeng Hao, Tony F. Heinz, James Hone, and Zhong Lin Wang. *Nature*, 514:470–474, 2014.
[41] Ruixiang Fei, Wenbin Li, Ju Li, and Li Yang. *Applied Physics Letters*, 107:173104, 2015.
[42] Pierre Labéguerie, Moussab Harb, Isabelle Baraille, and Michel Rérat. *Phys. Rev. B*, 81:045107, 2010.